

Large-scale structural reorganization of strange attractors

Christophe Letellier,¹ Tsvetelin D. Tsankov,² Greg Byrne,³ and Robert Gilmore⁴

¹*CORIA UMR 6614, Université de Rouen, BP 12, Av. de l'Université, Saint-Etienne du Rouvray cedex, France*

²*Physics Department, Bryn Mawr College, Bryn Mawr, Pennsylvania 19010-2899, USA*

³*Areté Associates, 1550 Crystal Drive, Arlington, Virginia 22202, USA*

⁴*Physics Department, Drexel University, Philadelphia, Pennsylvania 19104, USA*

(Received 4 February 2005; published 18 August 2005)

Strange attractors can exhibit bifurcations just as periodic orbits in these attractors can exhibit bifurcations. We describe two classes of large-scale bifurcations that strange attractors can undergo. For each we provide a mechanism. These bifurcations are illustrated in a simple class of three-dimensional dynamical systems that contains the Lorenz system.

DOI: [10.1103/PhysRevE.72.026212](https://doi.org/10.1103/PhysRevE.72.026212)

PACS number(s): 05.45.-a

I. INTRODUCTION

Strange attractors are generated by dynamical systems that depend on parameters. These are deterministic sets of first order nonlinear ordinary differential equations of the form $\dot{x}_i = f_i(x; c)$, where the state variables x_i define the state of the system and the control parameters c can be varied. State variables typically model physical variables (laser intensity, concentration of chemical species) and control variables typically model experimental conditions (laser pumping rates, chemical flow rates). As the control parameters c are varied strange attractors undergo changes. It is one of the goals of dynamical systems theory to understand and predict the spectrum of changes that a nonlinear dynamical system can undergo under parameter variations [1–5].

Some changes are simple and well known. These involve bifurcations of fixed points and of periodic orbits. Fixed point bifurcations are described by the theory of singularities [6–8]. The bifurcations that periodic orbits can undergo when a single parameter is varied include only period-doubling bifurcations and saddle-node bifurcations [1–5]. However, strange attractors themselves can undergo bifurcations as control parameters change. It is now possible to study the spectrum of bifurcations that strange attractors can undergo because of the structures that have been introduced to describe and classify strange attractors in three dimensions. As these bifurcations go beyond the bifurcations allowed to fixed points and periodic orbits, we call these kinds of bifurcations “perestroikas,” a term commonly used in catastrophe theory and the theory of singularities [6–9]. Perestroikas involve changes in the structures we use to characterize strange attractors. These are knot holders [4,5,10,11], which describe how the periodic orbits in a strange attractor are organized, and bounding tori [12,13], which describe how the knot holders themselves are organized.

Perestroikas that involve knot holders are encountered in the Rössler attractor. As control parameters change, branches can be added to (or removed from) the knot holder describing the strange attractor. In practical terms, this means that an additional symbol is required to uniquely label the unstable periodic orbits embedded in the strange attractor.

Perestroikas that involve bounding tori, and the knot holders within them, are encountered in the Lorenz attractor. As control parameters change the connectivity of the strange attractor can change. For example, a connected attractor can bifurcate to a symmetry-related pair of disconnected attractors, only one of which is seen for any initial condition. Proceeding in the opposite direction, two disconnected attractors can be joined by a “symmetry-restoring” bifurcation. These large-scale bifurcations occur in a limited number of ways that are systematically explained in terms of bounding tori, the flows through them, and the bifurcations they can undergo. It is the purpose of the present paper to describe large-scale structural reorganizations of strange attractors.

This paper is organized as follows. In Sec. II we review some of the tools that are important for the description of the global changes that strange attractors can undergo under parameter variation. In Sec. III we describe a known perestroika that occurs in the Rössler equations. We also introduce the ideas necessary to describe even larger-scale perestroikas. In Sec. IV we introduce a restricted class of familiar dynamical systems which exhibits this larger type of perestroika. In Sec. V we describe in general the mechanisms that lead to perestroikas of bounding tori, and in Sec. VI we show in detail how the mechanism occurs in the simple class of dynamical systems introduced in Sec. IV. The cases studied involve perestroikas between genus-one and genus-three strange attractors. In Sec. VII we discuss another related mechanism giving rise to large scale changes in the structure of strange attractors. This example occurs for the Lorenz attractor in a certain range of control parameter values. Results are summarized in Sec. VIII.

II. BACKGROUND

The properties of strange attractors are largely determined by the spectrum of unstable periodic orbits in the attractor and the topological organization of these orbits [1,3–5]. The organization is completely summarized by knot holders. They are called knot holders because they hold all the (unstable) periodic orbits in the strange attractor and describe the organization of these orbits [4,5,10,11]. Knot holders are

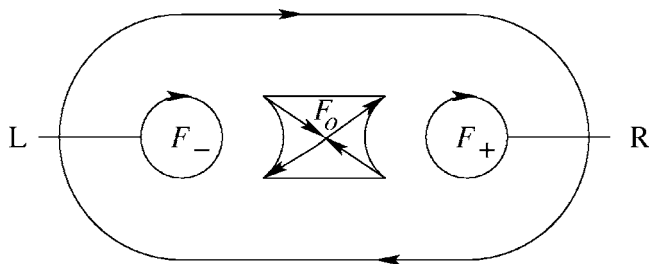


FIG. 1. Canonical form for the genus-3 bounding torus consists of an outer disk boundary and three interior holes. The four singularities on the boundary are confined to the central interior hole. Locations of the two disks (L,R) comprising the Poincaré surface of section are shown.

also called branched manifolds. The knot-holders themselves are highly constrained in the bifurcations they can undergo by bounding tori that enclose them. We briefly review the properties of branched manifolds and bounding tori.

A. Branched manifolds

Birman and Williams showed that it is possible to project a strange attractor that is contained in \mathbb{R}^3 onto a two-dimensional structure called a branched manifold [10,11]. This is done by projecting the flow down along the stable direction onto a surface defined by the expanding and the flow directions. This is made rigorous by identifying all points in the flow with the same future,

$$x \sim y \quad \text{if} \quad \lim_{t \rightarrow \infty} |x(t) - y(t)| = 0.$$

In this projection periodic orbits are neither created nor destroyed. Further, their topological organization remains unchanged since no self-intersections occur during this projection. As a result, the branched manifold can be used to identify the topological organization of all the unstable periodic orbits in the strange attractor. Since the unstable periodic orbits and their topological organization identify the strange attractor, this means that branched manifolds can be used to identify and classify strange attractors [14–16].

B. Bounding tori

Strange attractors and the branched manifolds that classify them can in turn be classified by their connectivity properties [12,13]. The easiest way to do this is to “blow up” or “inflate” the semiflow on the branched manifold to a flow in a neighborhood of the branched manifold that has the appropriate limiting properties. This bounded open set in \mathbb{R}^3 has a bounding surface. The surface is orientable, the inside contains the attractor. It is trapping, any orbit that passes through from outside to inside remains trapped inside forever. The surface is also bounded and closed. It is therefore a torus. All tori are identified by a single non-negative integer, the topological index called the genus, g , which is the number of holes in the boundary. The surface with $g=0$ is called a sphere and that with $g=1$ is commonly called a torus. The blow-up of the flow induces a flow on this boundary. Al-

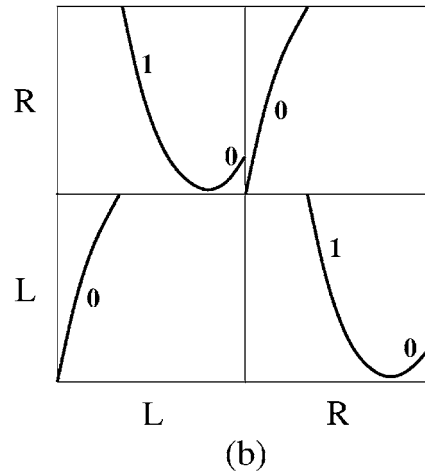
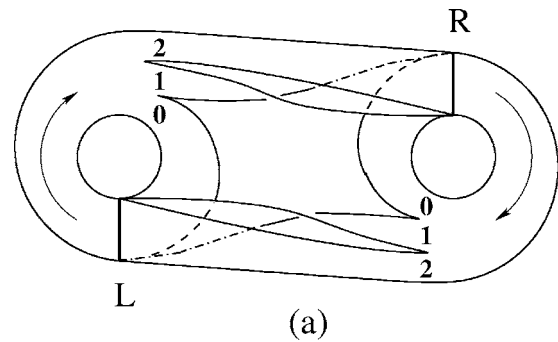


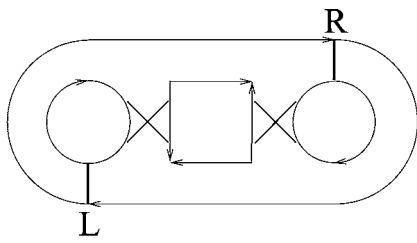
FIG. 2. (a) Branched manifold compatible with the bounding torus shown in Fig. 1. There are two branch lines and six branches, three from L labeled 0,1,2 and three from R labeled 0,1,2. (b) Return map for this branched manifold. Diagonal parts describe the $L \rightarrow L$ and $R \rightarrow R$ flows and off-diagonal parts describe the $L \rightarrow R$ and $R \rightarrow L$ flows. The local torsion $(0,1,0)$ is shown associated with each branch.

though the flow on the branched manifold has no fixed points in the open neighborhood of the branched manifold, when restricted to the surface there are fixed point singularities. All are saddles. As a result, the number of fixed points of the flow on the boundary is related to the genus, and this number is $2(g-1)$ [13].

The flow, restricted to the bounding torus surface, can be set into canonical form. For genus $g=0,1,2,3,4,5,6,7,8,\dots$ there are $0,1,0,1,1,2,2,5,6,\dots$ inequivalent canonical forms [13]. These forms can be uniquely identified by a symbol sequence (“periodic orbit”) of period $g-1$. The number of canonical forms increases exponentially with an entropy of $\ln(3)$ [17]. The canonical form for $g=3$ is shown in Fig. 1.

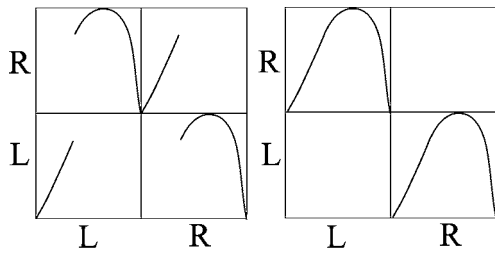
C. Global Poincaré surface of section

In three dimensions a Poincaré surface of section is a minimal two-dimensional surface with the property that all points in the attractor intersect this surface transversally an infinite number of times under the flow. The Poincaré surface of section need not be connected and in fact is often not connected. The urge to define Poincaré sections as connected surfaces has led to many problems in the past. In particular,

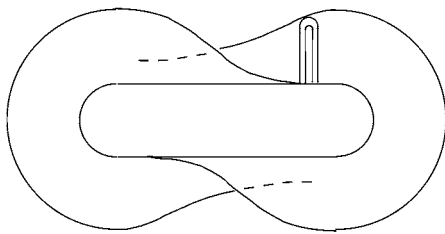


(a) Flow through the interior flow

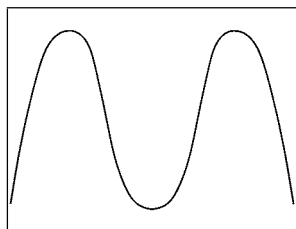
tubes is restricted.



(b) The return map becomes increasingly off-diagonal, finally off-diagonal in the limit that the flow through these two flow tubes is completely restricted.

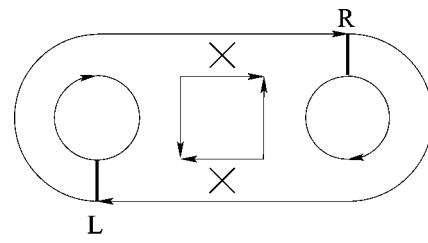


(c) The original attractor is deformed into a single attractor, with one branch line and $4 = 2^2$ branches, contained within a genus-1 bounding torus.

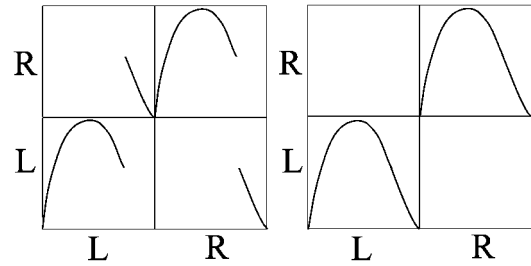


(d) The return map on the single branch line has four branches.

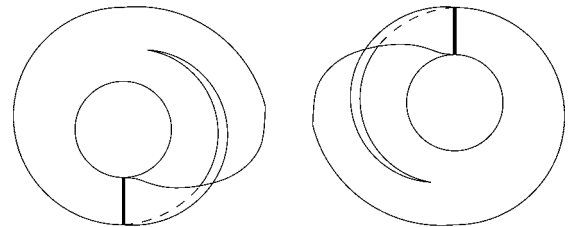
FIG. 3. One perestroika that can occur for the genus-3 bounding torus when the two interior flow tubes are restricted.



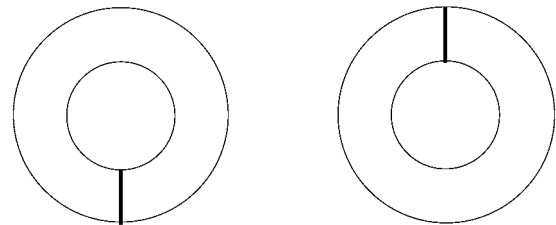
(a) Flow through the exterior flow tubes is restricted.



(b) The return map becomes increasingly diagonal, finally diagonal in the limit that the flow through these two flow tubes is completely restricted.



(c) The original strange attractor is deformed into two disjoint strange attractors



(d) Each attractor is in a genus-1 bounding torus, each with a single branch line.

FIG. 4. One perestroika that can occur for the genus-3 bounding torus when the two exterior flow tubes are restricted.

this point was addressed in the context of systems with various type of symmetries [18–22]. In fact, the Poincaré section is generally the disjoint union of nonoverlapping disks [12,13,23].

TABLE I. Coefficients of several quadratic systems with $\mathcal{R}_Z(\pi)$ symmetry.

System	X	Y	XZ	YZ	X	Y	XZ	YZ	Z	X^2	XY	Y^2	Z^2	Reference	
	a_1	a_2	a_3	a_4	b_1	b_2	b_3	b_4	c_0	c_1	c_2	c_3	c_4	c_5	
(1) Lorenz	$-\sigma$	$+\sigma$	0	0	R	-1	-1	0	0	$-b$	0	+1	0	0	[35]
(2) Chen and Ueta	$-\sigma$	$+\sigma$	0	0	$R-\sigma$	R	-1	0	0	$-b$	0	+1	0	0	[36]
(3) Wang, Singer, and Bau	$-\sigma$	$+\sigma$	0	0	0	-1	-1	0	Ra	-1	0	+1	0	0	[37]
(4) Shimizu and Morioka	0	+1	0	0	1	$-\mu$	-1	0	0	$-\alpha$	+1	0	0	0	[38]
(5) Rucklidge	0	+1	0	0	$-\lambda$	$+\kappa$	-1	0	0	-1	+1	0	0	0	[39]
(6) Lusseyran and Brancher	$-\alpha$	$\alpha\beta$	α	α	α	$-\alpha\gamma$	$-\alpha$	$-\alpha C$	0	$-\nu$	-1	-1	0	0	[40]
(7) Burke and Shaw	$-S$	$+S$	0	0	0	-1	$-S$	0	\mathcal{V}	0	0	$+S$	0	0	[41]
(8) Sprott B	$-\sigma$	σ	0	0	0	0	+1	0	b	0	0	-1	0	0	[42]
(9) Sprott C	$-\sigma$	$+\sigma$	0	0	0	0	+1	0	b	0	0	0	-1	0	[42]
(10) Rikitake	$-\mu$	0	0	+1	$-a$	$-\mu$	+1	0	+1	0	0	-1	0	0	[43]

The Poincaré surface for a genus-one bounding torus consists of a single disk that is transverse to the flow. The Poincaré surface for a canonical genus- g bounding torus consists of the union of $g-1$ disjoint disks. The locations of these disks are determined algorithmically [13]. The locations of the two disks for the genus-3 canonical form is shown in Fig. 1. They are labeled L and R .

D. Branch lines

Many different branched manifolds can be described by the same genus- g canonical form. Each branch line in any of these branched manifolds can be moved so that it is contained in one of the $g-1$ components of the global Poincaré surface of section. As a result, any branched manifold enclosed by a genus- g bounding torus has exactly $g-1$ branch lines (for $g > 1$).

E. Return maps

Return maps for branched manifolds enclosed by a genus-one bounding torus are well known. They are equivalent to maps from the single branch line that exists in the single component of the Poincaré section back to itself. That is, in this case return maps are exactly maps of the interval to itself. Simple continuity requirements ensure that all critical points are differentiable.

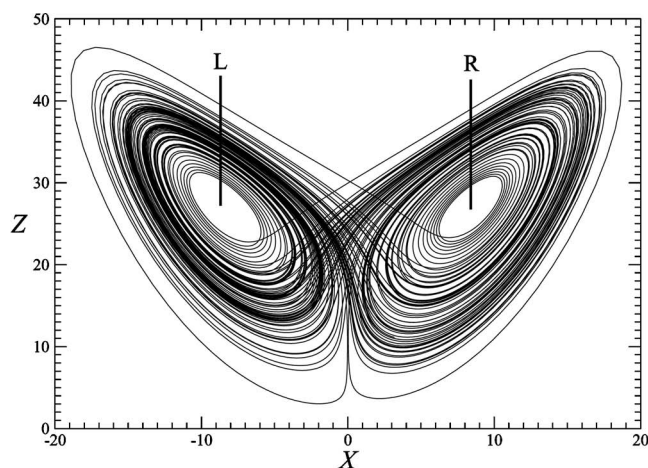
In the genus $g \geq 3$ case return maps can be constructed algorithmically [24]. There are $g-1$ branch lines. Initial conditions on any branch line flow to exactly two other branch lines. The return map is constructed as follows. Each branch line is represented as an interval. These are laid out along a horizontal axis (initial conditions). Each branch line can be oriented, from the interior to the exterior of the projection of the bounding torus onto a plane (cf. Fig. 1). As in the genus-one case, the images are arranged along the vertical axis. Over each point on the horizontal axis (consisting of $g-1$ disjoint oriented segments) there is a unique image. Each branch line has images in exactly two branch lines. Some return maps of this type are shown in Fig. 2(b) and Fig. 3(b).

F. Folding and tearing

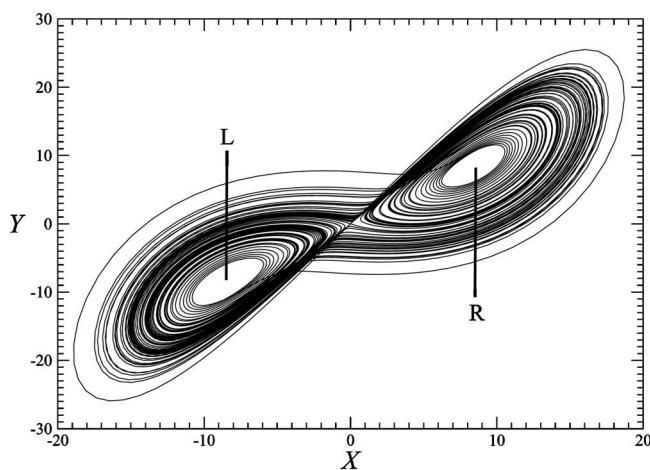
Return maps of a branch line onto itself in a genus-one bounding torus exhibit differentiable maxima and minima that reflect the folding that takes place between adjacent branches. In bounding tori with $g \geq 3$ initial conditions on any branch line flow to exactly two other branch lines. There is some point p along each branch line with the property that initial conditions on one side evolve to one branch line and initial conditions just to the other side evolve to a different branch line. This point is called a “tearing point” and is an initial condition for the flow into a saddle type singularity. At this point the return map exhibits a jump discontinuity and often a slope discontinuity as well. These discontinuities show that tearing takes place in the flow. Tearing occurs in the neighborhood of saddle points or other singularities that deflect the flow in a small neighborhood into divergent directions [24]. Folding and tearing are exhibited in the return map shown in Fig. 2(b).

G. Unfoldings of dynamical systems

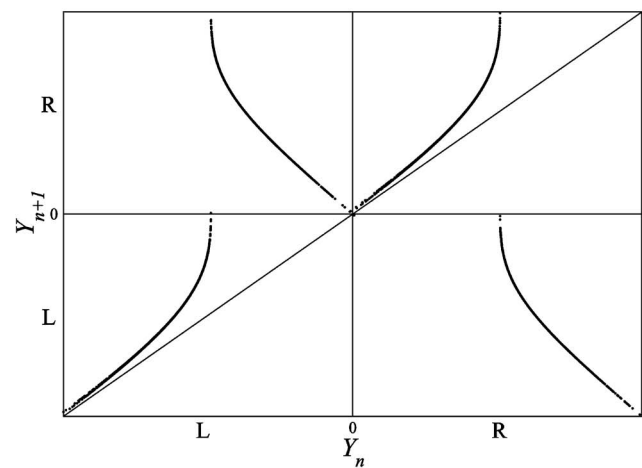
Most of the nonlinear dynamical systems that have been studied depend on only a small number of control parameters. The Rössler and Lorenz systems depend on three control parameters. The systems presented in Sec. IV depend on one, two, or three control parameters except for the sixth system in Table I, which depends on five. In the face of such a paucity of control parameters the full range of possible behaviors of these dynamical systems cannot be exhibited simply by varying the control parameters that are built into the model. This differs from the situation that exists in the study of catastrophes and singularities [6–9]. In these studies there is a procedure for constructing a “universal unfolding” of the singularity by adding perturbations that encapsulate all possible behaviors in a neighborhood of the singularity. There is no such theory for dynamical systems at the present time (except in the neighborhood of fixed points). Lacking such a theory, we are forced to the next best approach, which is topological in nature. In effect, we replace the (unknown) infinite dimensional universal perturbation of a dynamical system with a topological description of the system [4,5].



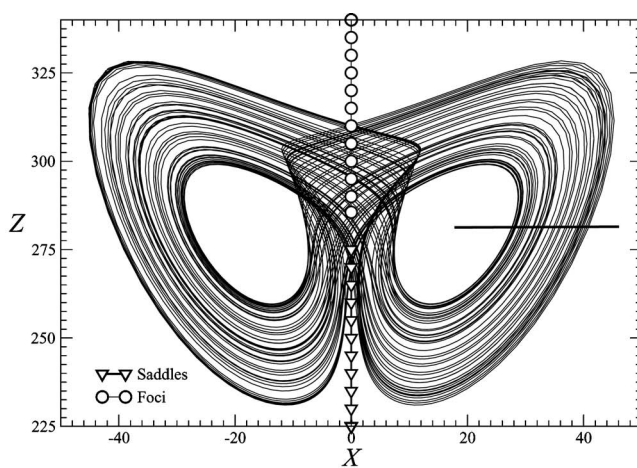
(a) X-Z plane projection



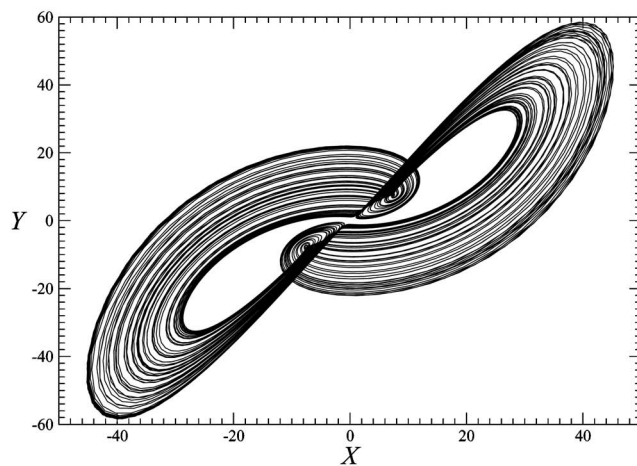
(b) X-Y plane projection



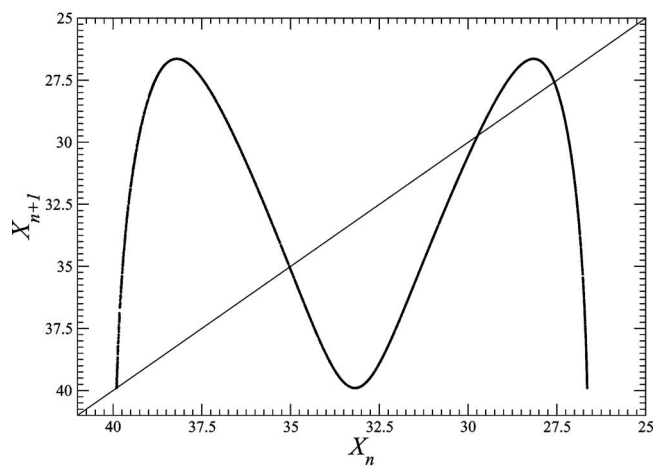
(c) First-return map



(a) X-Z plane projection



(b) X-Y plane projection



(c) First-return map

FIG. 5. Projection of the Lorenz attractor onto (a) the X-Z plane and (b) the X-Y plane. The two components of the global Poincaré section are shown. (c) Return map on the two branch lines shows that tearing occurs. Parameter values $(R, \sigma, b) = (28.0, 10.0, 8/3)$.

FIG. 6. Projection of the Lorenz attractor onto (a) the X-Z plane and (b) the X-Y plane. (c) First-return map to a single component Poincaré section shows that only folding occurs. Parameter values $(R, \sigma, b) = (278.56, 30.0, 1.0)$.

TABLE II. Control parameter values for which the symmetric dynamical systems generate strange attractors that exist in genus-1 and genus-3 bounding tori. All these systems have parameter values for which the attractor is associated with a folding and a tearing mechanism. Values reported are for genus-3 (tearing) and genus-1 (folding) attractors.

System	Parameters	Genus-3	Genus-1
(1) Lorenz	(R, σ, b)	(28.0, 10.0, 8/3)	(278.56, 30.0, 1.0)
(2) Chen and Ueta	(R, σ, b)	(22.05, 35.0, 5.0)	(35.0, 25.264, 1.0)
(3) Wang, Singer, and Bau	(R, σ)	(48.0, 10.0)	(128.0, 21.7)
(4) Shimizu and Morioka	(α, μ)	(0.375, 0.810)	(0.191457, 0.810)
(5) Rucklidge	(κ, λ)	(-2.0, -6.7)	(-4.4, -39.7)
(6) Lusseyran and Brancher	$(\alpha, \beta, \gamma, C, \nu)$	(1.01, 0.1136, 11.25, 93.5, 3.0)	(1.78, 0.1136, 11.25, 93.5, 0.0)
(7) Burke and Shaw	(S, \mathcal{V})	(0.85, 0.80)	(10.0, 4.271)
(8) Sprott B	(σ, b)		(2.73, 2.73)
(9) Sprott C	(σ, b)		(0.60, 0.045677)
(10) Rikitake	(α, μ, c)	(8.0, 2.7455, 1.0)	(8.0, 0.75, 1.0)

III. A KNOWN PERESTROIKA

Some perestroikas are familiar and others are less so. As control parameters are changed, in the Rössler equations [25],

$$\dot{x} = -y - z,$$

$$\dot{y} = x + ay,$$

$$\dot{z} = b + z(x - c), \quad (1)$$

for example, there is an alternation between chaotic and periodic behavior. The periodic behavior is seen in the form of periodic windows. In particular, as a control parameter changes a saddle node bifurcation can create a pair of periodic orbits, one of which is unstable and the other is initially stable. The stable periodic orbit “eats a hole” (window) in the bifurcation diagram, and undergoes period doubling to accumulation. Eventually a crisis closes the periodic window. For strange attractors generated by the Smale horseshoe mechanism, the partial order in which periodic orbits can be created on the way from laminar to chaotic behavior is constrained by topological considerations. Forcing diagrams for the simple Smale horseshoe exist to exhibit these constraints [5, 26–30].

In the perestroika just described, all the orbits can be identified by just two symbols, 0 and 1 $(a, b, c) = (0.432, 2, 4)$ [30]. A class of perestroikas occurs when orbits are created that require more than two symbols for their description using symbolic dynamics. For example, the symbol set $(0, 1)$ must be extended to $(0, 1, 2)$ to describe orbits in the Rössler attractor in a certain range of parameter values $0.432 < a < 0.492$. There is an entire sequence of perestroikas in which symbols are added [e.g., $(0, 1, 2) \rightarrow (0, 1, 2, 3)$] or removed [e.g., $(0, 1, 2, 3) \rightarrow (1, 2, 3)$] as control parameters are varied. These come about as the branched manifold that describes the strange attractor undergoes stretching and scrolling (see Figs. 7.36 and 7.45 in Ref. [5, 30, 31]).

Sometimes even more profound changes occur as control parameters are varied. These involve changes in the global topological structure of the attractor. Such perestroikas need not involve changes in the number of symbols required to identify each periodic orbit in the attractor. In fact, what changes is the connectivity properties of the strange attractor. To be more precise, what changes is the connectivity of the branched manifold that describes the strange attractor.

IV. CLASS OF SYSTEMS STUDIED

In order to exhibit these perestroikas, it is useful to study dynamical systems that create strange attractors that can be enclosed in genus-3 bounding tori. A useful collection of such strange attractors is generated by autonomous dynamical systems with a rotation $[\mathcal{R}_Z(\pi)]$ symmetry in \mathbb{R}^3 and with forcing terms of degree not exceeding two [32]. The most general form for flows with $\mathcal{R}_Z(\pi)$ symmetry is [33]

$$\frac{d}{dt} \begin{bmatrix} X \\ Y \\ Z \end{bmatrix} = \begin{bmatrix} F_{X,X} & F_{X,Y} & 0 \\ F_{Y,X} & F_{Y,Y} & 0 \\ 0 & 0 & F_Z \end{bmatrix} \begin{bmatrix} X \\ Y \\ 1 \end{bmatrix}. \quad (2)$$

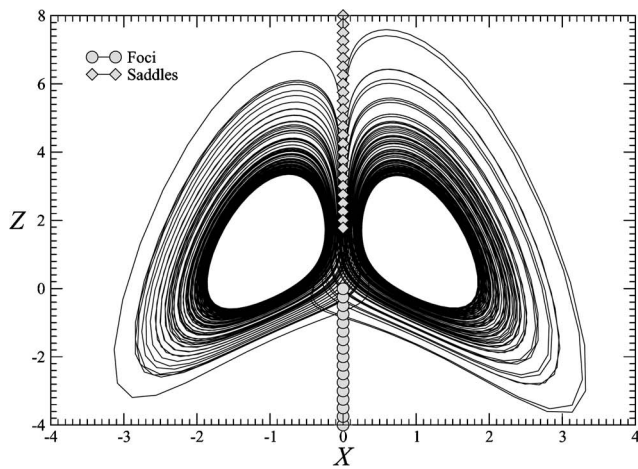
The five functions in the equation above are invariant under the actions of the group, so depend on the invariants X^2, XY, Y^2, Z . The most general dynamical system with $\mathcal{R}_Z(\pi)$ symmetry and forcing terms of degree no higher than two is

$$\dot{X} = a_1 X + a_2 Y + a_3 XZ + a_4 YZ,$$

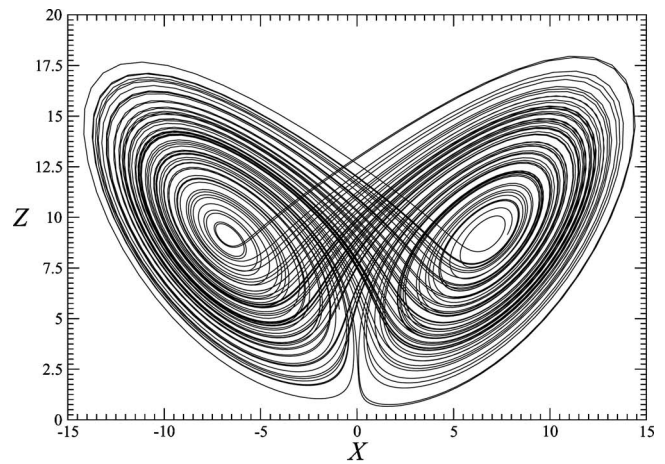
$$\dot{Y} = b_1 X + b_2 Y + b_3 XZ + b_4 YZ,$$

$$\dot{Z} = c_0 + c_1 Z + c_2 X^2 + c_3 XY + c_4 Y^2 + c_5 Z^2. \quad (3)$$

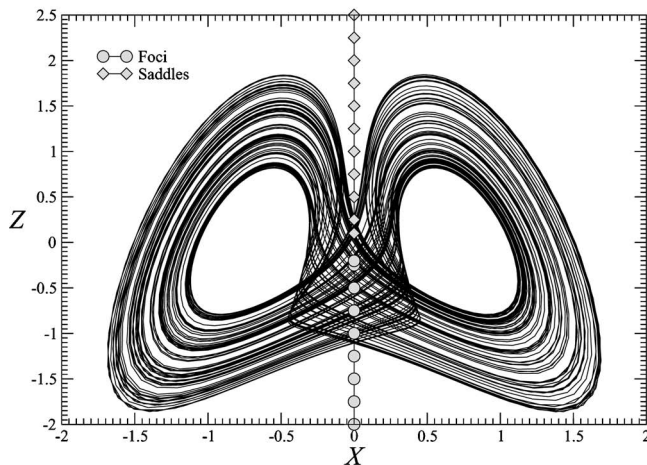
The values of the coefficients (a, b, c) for all the dynamical systems with these properties that have been studied are provided in Table I. Parameter values for different types of behavior are presented in Table II.



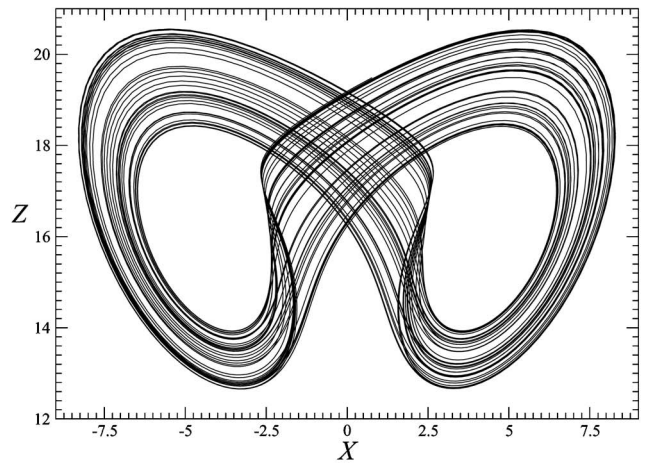
(a) Tearing: $(S, \mathcal{V}) = (0.85, 0.80)$



(a) Tearing: $(R, \sigma, b) = (22.05, 35, 5)$



(b) Folding: $(S, \mathcal{V}) = (10, 4.271)$



(b) Folding: $(R, \sigma, b) = (35, 25.264, 1)$

FIG. 7. Chaotic attractors for the Burke and Shaw system. (a) Attractor with a tearing mechanism occurs around the upper part of the Z axis which has the transverse stability of saddles. (b) Attractor with a folding mechanism occurs around the lower part of the Z axis which has the transverse stability of foci.

The large scale structure of a strange attractor is largely determined by the number, location, and stability of the co-existing fixed points.

The number of fixed points is governed by Bezout's theorem [34]. This theorem states that the number of fixed points of a set of polynomial equations is bounded above by the product of the degrees of these equations. In the present case, this is $d_x \times d_y \times d_z$, where d_x is the degree of the forcing terms in the equation $\dot{X} = f(X, Y, Z)$, etc. Since we are restricting ourselves to quadratic equations this product cannot exceed 8. In fact, for all except the sets of Eqs. (6) and (10), this product is 4.

The fixed points are of two types. They occur in symmetry-related pairs off the Z axis, and as twofold degenerate fixed points on the Z axis. Bezout's theorem counts the number of fixed points, including their degeneracy. For all of the systems in the table above, we choose control parameter

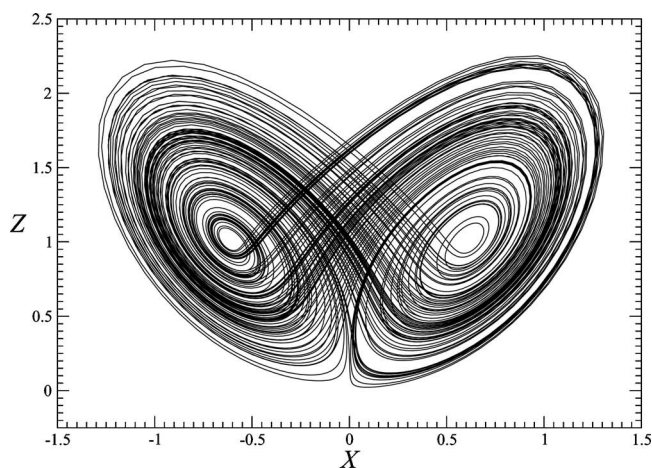
FIG. 8. Chaotic attractors for the Chen and Ueta system. (a) Attractor with a tearing mechanism contained in a bounding torus of genus-3 and (b) attractor with a folding mechanism contained in a bounding torus of genus-1.

values so that there are only two off-axis fixed points that are related by the symmetry, and they are unstable foci. The remaining fixed point, if it exists, must be on the Z axis. This fixed point exists at $(0, 0, Z)$, where Z is determined by $\dot{Z} = c_0 + c_1 Z + c_5 Z^2 = 0$. Since $c_5 = 0$ for all the systems listed in Table I, the fixed point occurs at $Z = -c_0/c_1$. For the systems (7)–(10) the fixed point is “at infinity” since $c_1 = 0$. That is, there is no fixed point. In the remaining cases [except case (3)] it is at 0 since $c_0 = 0$. In case (3) it occurs at $Z = Ra$.

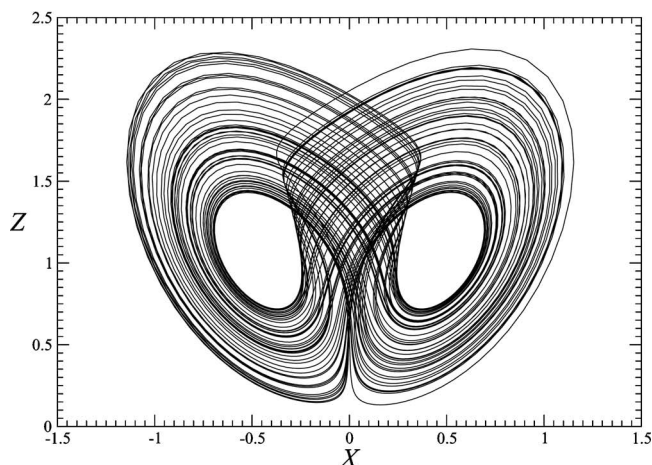
The global properties of the strange attractor are governed by the stability properties of the flow in the direction transverse to the Z axis. The stability matrix on the Z axis is

$$\begin{bmatrix} a_1 + a_3 Z & a_2 + a_4 Z & 0 \\ b_1 + b_3 Z & b_2 + b_4 Z & 0 \\ 0 & 0 & c_1 + 2c_5 Z \end{bmatrix}. \quad (4)$$

From this it is clear that the eigenvectors are along and orthogonal to the symmetry axis, and the eigenvalue in the Z



(a) Tearing: $\alpha = 0.375$



(b) Folding: $\alpha = 0.191457$

FIG. 9. Chaotic attractors for the Shimizu and Morioka system with $\mu=0.810$. (a) Tearing mechanism within a torus of genus-3 and (b) folding mechanism within a genus-1 torus.

direction is $c_1 + 2c_5Z$. For systems (7)–(10) the Z axis is invariant with constant nonzero flow $\dot{Z}=c_0$ along this axis.

The two other eigenvectors of the stability matrix are orthogonal to the Z axis. Their eigenvalues are determined by the 2×2 submatrix in (4). These eigenvalues determine to a large extent the global topology of the strange attractors (their genus) and the perestroikas they undergo.

V. PERESTROIKAS OF BOUNDING TORI

A bounding torus of genus-3 is shown in Fig. 1 [12,13]. This figure actually shows the projection of the two-dimensional surface of the genus-3 torus onto a two-dimensional plane. This projection consists of an outer boundary and three interior holes. The flow directions along all components of this surface are indicated by the arrows. The flows along the outer disk boundary and the two interior holes (shown round) on the left and right are in the same

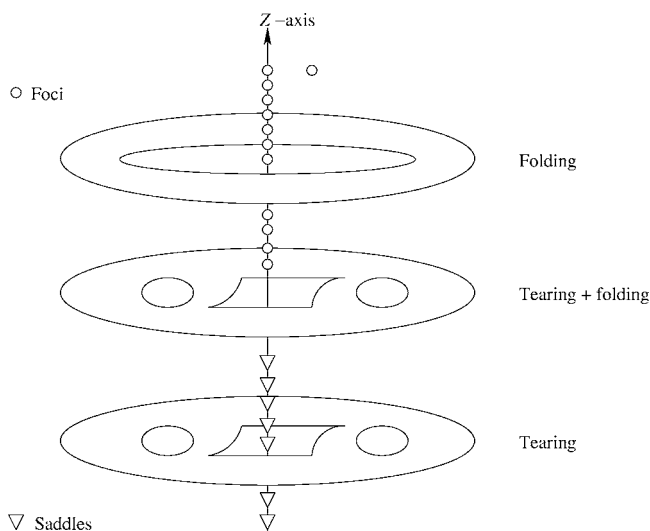
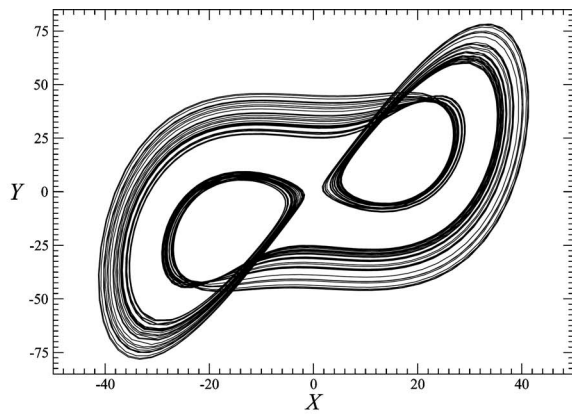


FIG. 10. As control parameters vary the attractor flows past the Z axis in different regions. Folding occurs when the transverse stability is that of a focus and tearing occurs when the transverse stability is that of a saddle. Both occur in the transition region.

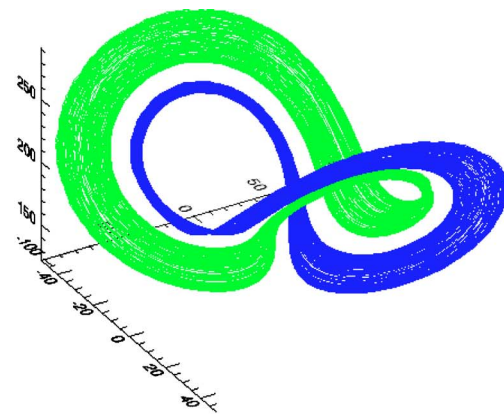
direction. The direction of the flow in the middle interior hole (shown square) changes direction at the four singularities. The direction of the flow at any interior point can be determined by continuity considerations. Since the genus is 3, the global Poincaré surface of section is the union of two disjoint disks that are transverse to the flow. The locations of these disks are shown as heavy lines extending between the interior round holes and the exterior boundary in Fig. 1.

Many distinct branched manifolds can exist within the surface of this bounding torus. For any such branched manifold, each branch line can be moved to a disk in the global Poincaré surface of section. All branched manifolds compatible with this bounding torus therefore have two branch lines. One such branched manifold is shown in Fig. 2(a). This branched manifold has six branches, two branch lines, and a twofold rotation symmetry. The three branches emanating from branch line L are labeled 0,1,2 (from inside to outside), and similarly from R . The return map for this branched manifold is shown in Fig. 2(b). The two branch lines are labeled L and R . Initial conditions on L are shown along the horizontal segment L and their images under the flow are shown above the initial condition. Initial conditions near the “inside” [see Fig. 2(a)] return to L and those nearer the outside flow to R . The branch labeled 0 connecting L to L has no torsion. The two branches labeled 1 and 2 that connect L to R have torsions of π and 0 radians. Each of the three branches of the return map over branch line L is labeled by the local torsion of the branch in the knot holder, 0,1,0. This return map shows that tearing occurs between branches 0 and 1, while folding occurs between branches 1 and 2. Initial conditions from branch line R are described in the same fashion [24].

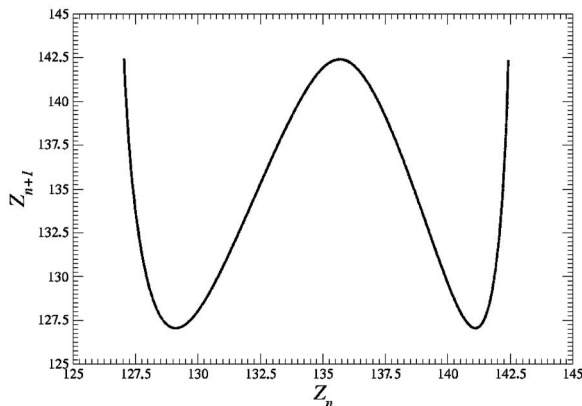
As control parameters change the strange attractor also changes. Small changes include creation and/or annihilation of periodic orbits. Larger changes include inclusion of additional branches or removal of branches already present. For example, the branches 2 ($L \rightarrow R$ and $R \rightarrow L$) may shrink until



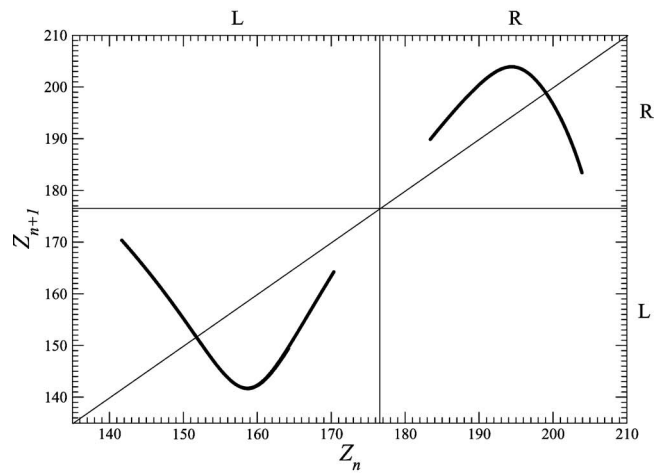
(a) Lorenz attractor



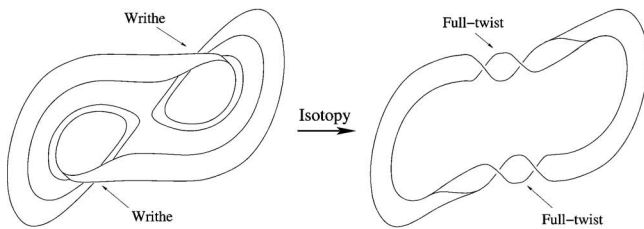
(a) Two linked attractors



(b) Return map on the branch line



(b) Their return maps



(c) Template

FIG. 11. Lorenz attractor after the saddle fails to split the flow, deflecting it to a single region in the state space. The attractor can be bounded by a genus-1 torus, so only one branch line is necessary. (c) The local torsion can be determined by an isotopy that exchanges writhe for twist. Parameter values $(R, \sigma, b) = (142.245, 10, 8/3)$.

the flow no longer goes through them, or these branches may grow until they reach an extremum and turn around, creating branches (“3”). In all these cases the two branch lines remain present and serve to feed more or fewer branches and the branched manifold remains bounded by a genus-3 bounding torus. (See Table II.)

The bounding tori can themselves experience perestroikas. We sketch the general arguments as they apply to a genus-3 bounding torus. For simplicity, we assume the flow satisfies a rotation symmetry $[\mathcal{R}_Z(\pi)]$. However, none of the

FIG. 12. (Color online) (a) Two linked genus-1 strange attractors generated by the Lorenz equations and (b) their return maps. Parameter values $(R, \sigma, b) = (207, 10, 8/3)$.

results described below depends on symmetry. As control parameters change the flow through some of the flow tubes in a bounding torus can be restricted and finally annihilated.

In Fig. 3(a) we show one perestroika that can occur for the genus-3 bounding torus. In this case the flow is restricted in the two interior flow tubes, marked with an \times . Flow in these tubes, when unrestricted, returns from L to L or from R to R . As the flow is restricted, the return map becomes increasingly “off diagonal,” and finally completely off diagonal, as shown in Fig. 3(b) [24]. In this case all initial conditions on L flow to R and those on R flow to L . This determinism means that one of the two components of the global Poincaré surface of section is redundant. This is consistent with the flow being contained in a genus-1 bounding torus. In this case the strange attractor with $4 = 2 \times 2$ branches and two branch lines in the genus-3 bounding torus is deformed and is now embedded in a genus-1 bounding torus. The branched manifold has a single branch line and $4 = 2^2$ branches. It is shown in Fig. 3(c). The return map on the single branch line (R) is shown in Fig. 3(d).

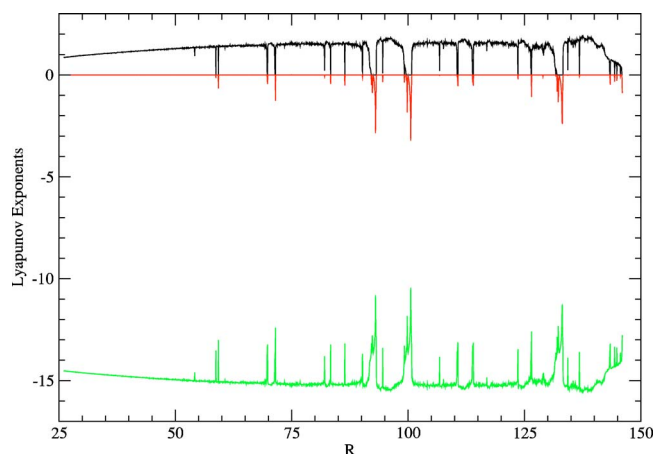


FIG. 13. (Color online) Lyapunov exponents for Lorenz attractor with $(\sigma, b) = (10.0, 8/3)$. The plots show no evidence that a global bifurcation occurs at $R = 142.026$.

In Fig. 4(a) we show what happens when the flow through the two exterior flow tubes marked with an \times , that carry the flow from one component of the Poincaré section to the other, is restricted. The return map becomes “more diagonal,” and finally diagonal [Fig. 4(b)] when the flow through these two flow tubes is completely cut off. The flow returns from branch line L to branch line L , or from R back to R . The strange attractor is “severed” into two components, each described by a branched manifold with one branch line. Each of these two branched manifolds is enclosed in a genus-1 bounding torus. This perestroika generates two genus-1 bounding tori from one genus-3 bounding torus. These are shown in Fig. 4(d). The branched manifolds within each are shown in Fig. 4(c). In this perestroika, a connected genus-3 attractor is transformed to two disjoint genus-1 attractors. The two bounding tori, and any strange attractors in them, are disjoint and unlinked. Such a scenario was observed in the twofold cover of the Rössler system [33].

VI. MECHANISM CAUSING PERESTROIKAS

Figures 5 and 6 show that the Lorenz attractor undergoes a perestroika as the control parameters change from $(R, \sigma, b) = (28.0, 10.0, 8/3)$ to $(278.56, 30.0, 1.0)$. The perestroika is described by a transition from a genus-3 bounding torus to a genus-1 bounding torus. During this change of control parameter values there is no change in the stability properties of the three fixed points but the locations of the two foci change.

The change occurs because changing the control parameter values forces the flow to visit different neighborhoods of the Z axis. For $(R, \sigma, b) = (28.0, 10.0, 8/3)$ the flow passes near the Z axis for small values of Z ($0 < Z < 30$). In this range of Z values the Z axis has the transverse stability of a saddle. The saddle structure of the Z axis splits the flow and is responsible for the tearing that is evident in the first return map, shown in Fig. 5(c). For $(R, \sigma, b) = (278.56, 30.0, 1.0)$ the flow passes around the Z axis for much larger values of Z ($275 < Z < 325$). In this range of Z values the transverse

stability is that of a focus. The transverse stability of this axis is shown clearly in Fig. 6(a). The projection of the strange attractor onto the X - Y plane [Fig. 6(b)] shows clearly that its bounding torus has genus-1, and the first return map [Fig. 6(c)] shows that no tearing occurs.

This mechanism operates to cause a genus-3 to genus-1 perestroika in the other dynamical systems presented in Table I. The strange attractors of genus-3 type and genus-1 type are shown for the Burke and Shaw dynamical system [41] in Fig. 7, the Chen and Ueta dynamical system [36] in Fig. 8, and the Shimizu-Morioka dynamical system [38] in Fig. 9.

Figure 10 provides a schematic representation of this mechanism. When the control parameter values cause the flow to pass the Z axis in a neighborhood where it has the transverse stability of a focus, only folding occurs and the attractor can be enclosed in a genus-1 torus. When the flow passes the Z axis in a neighborhood where it has the transverse stability of a saddle, tearing occurs and the attractor can be enclosed in a genus-3 torus. In the transition region both folding and tearing occur, as illustrated in the middle of Fig. 10. As long as tearing occurs, the attractor is enclosed in a genus-3 surface. We point out that the perestroika is not driven by change of stability of the fixed point on the Z axis (when there is one), or even the existence of a fixed point on the Z axis [cf. Table I, systems (7)–(10)], only by the transverse stability properties of the Z axis where the flow approaches it. The mechanism shown in Fig. 10 is responsible for creating the genus-3 to genus-1 perestroikas of the type shown in Fig. 3, where flow through the two interior flow tubes is restricted and finally annihilated.

VII. OTHER MECHANISMS

Mechanisms for creating perestroikas of the type shown in Fig. 4 have also been observed. In these mechanisms flow through the exterior flow tubes is restricted and finally annihilated. The result is a pair of symmetry-related strange attractors, each of genus-1 type.

Another mechanism can create a pair of symmetry-related strange attractors that are linked. The mechanism that generates this perestroika occurs in the Lorenz system. It can be considered in two steps. First, the control parameters are changed from $(R, \sigma, b) = (28.0, 10.0, 8/3)$ to values for which a genus-1 strange attractor exists. The attractor at $(R, \sigma, b) = (142.245, 10.0, 8/3)$ is shown in Fig. 11(a). Its return map on a global Poincaré surface of section is shown in Fig. 11(b). The attractor has four branches and a global torsion of $+2$. The global torsion is determined by the self-relative rotation rates of the unstable periodic orbits in the attractor. It can also be identified by carrying out the isotopic deformation shown in Fig. 11(c). This smooth transformation converts writhe to twist, or torsion.

A mechanism leading to a perestroika is illustrated in Fig. 11(b) and Fig. 12(b) in terms of return maps. Figure 11(b) shows a return map for a strange attractor that can be enclosed in a genus-1 bounding torus. In this return map the internal branch with positive slope has an even local torsion, $2n$. The two outer branches with negative slope have local

torsion $2n \pm 1$. If the control parameters are varied to generate the return map shown in Fig. 12(b), the attractor becomes disconnected. The two disconnected pieces have linking number n and are unlinked if $n=0$. Two linked attractors satisfying the Lorenz equations are shown in Fig. 12(a). Each of the two disconnected attractors contains one period-1 orbit according to the return map. The strange attractors have linking number 1 with each other. Such a scenario was also observed in the Burke and Shaw system [20] and in the simplest equivariant jerk system [44].

VIII. SUMMARY AND CONCLUSIONS

As experimental conditions or control parameters change, strange attractors also change. The changes can be described by a hierarchy with three levels of structure. At the first level is the set of unstable periodic orbits in the attractor. At the next level of structure are the branched manifolds that describe the unstable periodic orbits in the strange attractor. Branched manifolds can metamorphose by the addition of branches or the deletion of branches as control parameters vary. At the grossest level in this hierarchy, the bounding tori that enclose the branched manifolds can change. In this work we have described some changes that can occur and exhibited mechanisms responsible for bounding tori perestroikas in a large class of simple dynamical systems. This special class exhibits a rotation symmetry $[\mathcal{R}_z(\pi)]$, but the mechanism operates when the symmetry is broken or absent.

In general, the mechanism involves restricting the flow through either interior (Fig. 3) or exterior (Fig. 4) flow tubes of a bounding torus, with the following consequences:

Restriction	Initial	Final
Interior flow tube	genus-3 \rightarrow	genus-1
Exterior flow tube	genus-3 \rightarrow	$2 \times$ genus-1

The two genus-1 bounding tori, and the strange attractors enclosed by them, are not linked.

We exhibited another mechanism in which a strange attractor enclosed in a genus-1 bounding torus bifurcates to a pair of strange attractors. Each is enclosed in a genus-1 bounding torus, and the two tori are linked with nonzero linking number n . The Lorenz equations exhibit a perestroika of this type. It can be summarized as

$$\text{genus-3} \rightarrow \text{genus-1} \rightarrow 2 \times \text{genus-1}(\text{linked}).$$

Large scale structural reorganizations are neither predicted by nor correlated with changes in local dynamical or geometrical properties of strange attractors, such as Lyapunov exponents or generalized dimensions. This can be seen, for example, in Fig. 13, which is a plot of the Lyapunov exponents of the Lorenz attractor for $(\sigma, b) = (10.0, 8/3)$ in the range $26.0 \leq R \leq 148.0$. The global bifurcation occurs at $R=142.026$. This plot of the Lyapunov exponents clearly shows regions where stable periodic windows exist, but there are no indications at all that global bifurcations take place for any particular value of R .

ACKNOWLEDGMENTS

This work was partly done during a stay by C.L. at Drexel University. This work was supported in part by NSF Grant No. PHY9987468.

-
- [1] N. B. Tufillaro, T. Abbott, and J. Reilly, *An Experimental Approach to Nonlinear Dynamics and Chaos* (Addison-Wesley, Reading, MA, 1992).
 - [2] E. Ott, *Chaos in Dynamical Systems* (Cambridge University Press, Cambridge, 1993).
 - [3] H. G. Solari, M. A. Natiello, and G. B. Mindlin, *Nonlinear Dynamics: A Two-Way Trip from Physics to Math* (IOP, London, 1996).
 - [4] R. Gilmore, *Rev. Mod. Phys.* **70**, 1455 (1998).
 - [5] R. Gilmore and M. Lefranc, *The Topology of Chaos* (Wiley, New York, 2002).
 - [6] V. I. Arnol'd, S. M. Gusein-Zade, and A. N. Varchenko, *Singularities of Differentiable Mappings I* (Birkhäuser, Basel, 1985).
 - [7] R. Gilmore, *Catastrophe Theory for Scientists and Engineers* (Wiley, New York, 1981).
 - [8] V. I. Arnol'd, *Catastrophe Theory*, 2nd ed. (Springer-Verlag, New York, 1986).
 - [9] T. Poston and I. N. Stewart, *Catastrophe Theory and its Applications* (Pitman, London, 1978).
 - [10] J. Birman and R. F. Williams, *Topology* **22**, 47 (1983).
 - [11] J. Birman and R. F. Williams, *Contemp. Math.* **20**, 1 (1983).
 - [12] T. D. Tsankov and R. Gilmore, *Phys. Rev. Lett.* **91**, 134104 (2003).
 - [13] T. D. Tsankov and R. Gilmore, *Phys. Rev. E* **69**, 056206 (2004).
 - [14] N. B. Tufillaro, H. G. Solari, and R. Gilmore, *Phys. Rev. A* **41**, 5717 (1990).
 - [15] G. B. Mindlin, X.-J. Hou, H. G. Solari, R. Gilmore, and N. B. Tufillaro, *Phys. Rev. Lett.* **64**, 2350 (1990).
 - [16] G. B. Mindlin, H. G. Solari, M. A. Natiello, R. Gilmore, and X.-J. Hou, *J. Nonlinear Sci.* **1**, 147 (1991).
 - [17] J. Katriel and R. Gilmore (unpublished).
 - [18] C. Letellier and G. Gouesbet, *Phys. Rev. E* **49**, 3492 (1994).
 - [19] C. Letellier and G. Gouesbet, *Phys. Rev. E* **52**, 4754 (1995).
 - [20] C. Letellier, P. Dutertre, J. Reizner, and G. Gouesbet, *J. Phys. A* **29**, 5359 (1996).
 - [21] C. Letellier and G. Gouesbet, *J. Phys. II* **6**, 1615 (1996).
 - [22] C. Letellier, G. Gouesbet, and N. Rulkov, *Int. J. Bifurcation Chaos Appl. Sci. Eng.* **6**, 2531 (1996).
 - [23] T. D. Tsankov, A. Nishtala, and R. Gilmore, *Phys. Rev. E* **69**, 056215 (2004).
 - [24] G. Byrne, R. Gilmore, and C. Letellier, *Phys. Rev. E* **70**, 056214 (2004).
 - [25] O. E. Röessler, *Phys. Lett.* **57A**, 397 (1976).
 - [26] G. B. Mindlin, R. Lopez-Ruiz, H. G. Solari, and R. Gilmore, *Phys. Rev. E* **48**, 4297 (1993).
 - [27] T. Hall, *Phys. Rev. Lett.* **71**, 58 (1993).

- [28] T. Hall, *Nonlinearity* **7**, 861 (1994).
- [29] M. A. Natiello and H. G. Solari, *J. Knot Theory Ramif.* **3**, 511 (1994).
- [30] C. Letellier, P. Dutertre, and B. Maheu, *Chaos* **5**, 271 (1995).
- [31] R. Gilmore and X. Pei, "The topology and organization of unstable periodic orbits in Hodgkin-Huxley models of receptors with subthreshold oscillations," in *Handbook of Biological Physics, Vol. 4, Neuro-informatics, Neural Modeling*, edited by F. Moss and S. Gielen (North-Holland, Amsterdam, 2001), pp. 155–203.
- [32] R. Miranda and E. Stone, *Phys. Lett. A* **178**, 105 (1993).
- [33] C. Letellier and R. Gilmore, *Phys. Rev. E* **63**, 016206 (2000).
- [34] D. A. Cox, J. B. Little, and D. O'Shea, *Ideals, Varieties, and Algorithms* (Springer-Verlag, New York, 1996).
- [35] E. N. Lorenz, *J. Atmos. Sci.* **20**, 130 (1963).
- [36] G. Chen and T. Ueta, *Int. J. Bifurcation Chaos Appl. Sci. Eng.* **9**, 1465 (1999).
- [37] Y. Wang, J. Singer, and H. H. Bau, *J. Fluid Mech.* **237**, 479 (1992).
- [38] T. Shimizu and N. Morioka, *Phys. Lett.* **76A**, 201 (1980).
- [39] A. M. Rucklidge, *J. Fluid Mech.* **237**, 209 (1992).
- [40] F. Lusseyran and J. P. Brancher, *IEEE Trans. Magn.* **26**, 2875 (1990).
- [41] R. Shaw, *Z. Naturforsch. A* **36A**, 80 (1981).
- [42] J. S. Sprott, *Phys. Rev. E* **50**, R647 (1994).
- [43] T. Rikitake, *Proc. Cambridge Philos. Soc.* **54**, 89 (1958).
- [44] C. Letellier and J.-M. Malasoma, *Phys. Rev. E* **64**, 067202 (2001).